

# High-Efficiency Thermoelectrics with Functionalized Graphene

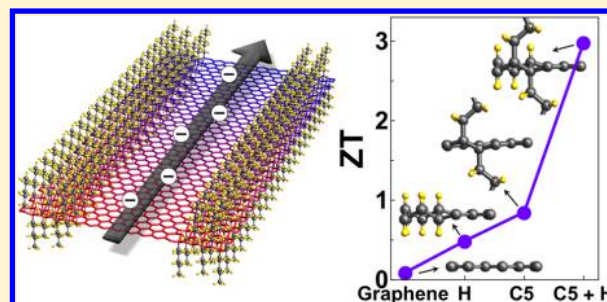
Jeong Yun Kim and Jeffrey C. Grossman\*

Department of Materials Science and Engineering, Massachusetts Institute of Technology, Cambridge, Massachusetts 02139, United States

## S Supporting Information

**ABSTRACT:** Graphene superlattices made with chemical functionalization offer the possibility of tuning both the thermal and electronic properties via nanopatterning of the graphene surface. Using classical and quantum mechanical calculations, we predict that suitable chemical functionalization of graphene can introduce peaks in the density of states at the band edge that result in a large enhancement in the Seebeck coefficient, leading to an increase in the room-temperature power factor of a factor of 2 compared to pristine graphene, despite the degraded electrical conductivity. Furthermore, the presence of patterns on graphene reduces the thermal conductivity, which when taken together leads to an increase in the figure of merit for functionalized graphene by up to 2 orders of magnitude over that of pristine graphene, reaching its maximum  $ZT \sim 3$  at room temperature according to our calculations. These results suggest that appropriate chemical functionalization could lead to efficient graphene-based thermoelectric materials.

**KEYWORDS:** graphene, chemical functionalization, transport, thermoelectrics



Recent progress in enhancing the figure of merit for thermoelectric materials has relied on a range of innovative strategies, including reduction of the dimensionality,<sup>1–3</sup> use of complex bulk materials,<sup>4,5</sup> or introduction of impurity states in the bulk phase.<sup>6,7</sup> These advances, based on modifications to three-dimensional (3D) crystalline materials, have been enabled by a deep understanding of the key thermoelectric (TE) properties such as thermal and electronic transport, and the impact of structural and chemical changes on these properties, in turn providing new design strategies for high-efficiency TE materials. In contrast to the case of 3D materials, two-dimensional (2D) materials such as graphene, single-layer boron nitride, or molybdenum disulfide have received little attention regarding their potential for thermoelectric applications. Given the fact that 2D materials are “all-surface,” any modification to their environment or chemical functionalization will be expected to have enormous impact on properties, an appealing attribute when faced with such constrained optimization problems as in the case of thermoelectrics. Chemical functionalization, in particular, plays a key role for both thermal and electronic transport in 2D materials because either all or nearly all atoms in the system can be functionalized, leading to large modifications of charge carriers<sup>8</sup> and phonon modes;<sup>9</sup> this is in contrast to the 3D case, where surface chemical functionalization has a much smaller impact on transport. Although such potentially controllable transport in 2D is appealing for thermoelectric applications, a unified understanding of the key TE properties in 2D materials is needed in order to assess the potential of 2D TE and to provide design strategies for increasing the efficiency of this new class of TE materials.

Recent work has shown that the most familiar 2D carbon material, namely graphene, exhibits remarkable electronic transport properties, with a record carrier mobility of  $\sim 200\,000\text{ cm}^2\text{ V}^{-1}\text{ s}^{-1}$  reported for a suspended single layer<sup>10</sup> as well as a moderate Seebeck coefficient ( $S$ ) of  $\sim 80\text{ }\mu\text{V K}^{-1}$ .<sup>11,12</sup> Graphene is well known to possess an ambipolar nature, such that the sign of  $S$  can be controlled by changing the gate bias instead of doping.<sup>13</sup> Experimentally measured values of the thermoelectric figure of merit ( $ZT$ ) for pristine graphene at room temperature are in the range of 0.1–0.01,<sup>11,12,14,15</sup> roughly 2 orders of magnitude lower than the most efficient 3D thermoelectric materials such as  $\text{Bi}_2\text{Te}_3$  alloys.<sup>16</sup> Such low  $ZT$  values for graphene are to be expected due to its extremely high thermal conductivity ( $\kappa$ ), on the order of  $2000\text{--}5000\text{ W m}^{-1}\text{ K}^{-1}$ .<sup>15,17,18</sup> As mentioned above, graphene can be modified controllably with chemical functionalization, which in turn modulates its electronic and thermal transport properties; a range of methods have been employed to fabricate graphene heterostructures, for example, hydrogen functionalization,<sup>19</sup> introduction of in-sheet regions of hexagonal boron nitride (h-BN),<sup>20</sup> or the attachment of polymers using patterning processes such as lithography.<sup>21</sup> These controllable patterning techniques facilitate routes to the formation of a range of confined graphene patterns, including dots, lines, and more complex structures, within a single sheet of graphene.

Received: November 5, 2014

Revised: March 23, 2015

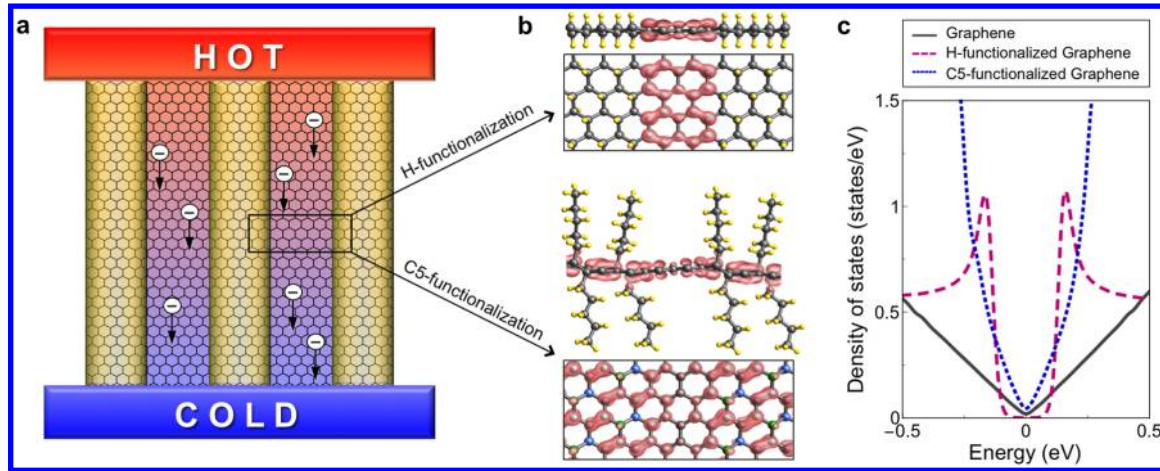


**Figure 1.** (a) Schematic of 2D thermoelectric based on patterned graphene nanoroads with an armchair-type boundary. Yellow shaded area indicates the patterned region. (b) H-functionalized graphene (HG) for 6 Å pattern width (top) and C5-functionalized graphene (CSG) (bottom). C and H atoms are represented by gray and yellow spheres, respectively. Pink contour plot represents charge density of the conduction band in each sample. Green and blue spheres indicate the C sites where C5 chains are attached on the up and down side of graphene, respectively. (c) Density of states (DOS) per unit cell of graphene, HG and CSG.

In this work, we consider the prospect of patterned graphene nanoroads<sup>22</sup> as an efficient thermoelectric material. The patterning introduces quantum confinement in pure (unfunctionalized) graphene by reducing its dimensionality from 2D to quasi-1D, with the periodic functionalization lines forming arrays of parallel graphene regions. Confinement in the material leads to an improvement in the power factor by increasing the density of states at the Fermi level, as demonstrated in recent studies<sup>1–3</sup> for low-dimensional thermoelectric materials. Here, ab initio electronic structure calculations and the Boltzmann transport approach are used to determine the role of such functionalization on the electrical transport properties, including the electrical conductivity ( $\sigma$ ) and Seebeck coefficient ( $S$ ), which combined with our computed thermal conductivities enables us to predict the full ZT in these materials. Our results show that ZT can reach values as high as 3 at room temperature, and demonstrate the potential for controllably tuning the properties of 2D materials for thermoelectric applications.

**Methodology.** Room-temperature transport calculations of patterned graphene nanoroads are carried out using electronic structure calculations and the Boltzmann transport approach. First-principles calculations are performed within the framework of density functional theory (DFT) as implemented in the plane-wave basis VASP code.<sup>23</sup> The projected augmented wave pseudopotentials<sup>24</sup> with the PW91<sup>25</sup> generalized gradient approximation of Perdew and Wang is used for treatment of the exchange-correlation energy. Geometry optimizations are performed using the conjugate gradient scheme until force components on every atom are less than 0.01 eV Å<sup>-1</sup>. The fully relaxed structures are used to compute the electronic band structure.

Transport coefficients are calculated by employing semiclassical Boltzmann theory within the constant relaxation time approximation, as implemented in the BOLTZTRAP code.<sup>26</sup> The electrical conductivity and Seebeck coefficient are calculated by defining the following function

$$L^{(\alpha)} = e^2 \sum_n \int \frac{d\mathbf{k}}{4\pi^3} \left( -\frac{\partial f(\epsilon_{n\mathbf{k}})}{\partial \epsilon_{n\mathbf{k}}} \right) \tau_n(\epsilon_{n\mathbf{k}}) v_{n\mathbf{k}} v_{n\mathbf{k}} (\epsilon_{n\mathbf{k}} - \mu)^\alpha \quad (1)$$

where  $e$  is the electronic charge,  $\tau_n$  the energy-dependent relaxation time,  $v_{n\mathbf{k}} = (1/\hbar) \nabla_{\mathbf{k}} \epsilon_{n\mathbf{k}}$  the group velocity in the  $n$ th band at  $\mathbf{k}$ ,  $\epsilon_{n\mathbf{k}}$  the energy eigenvalues obtained from DFT,  $\mu$  the chemical potential, and  $f(\epsilon_{n\mathbf{k}})$  the Fermi–Dirac function at a given temperature  $T$ . Here, we are interested in transport along the pattern direction ( $y$ ), which is obtained from  $\sigma = L_{yy}^{(0)}$  and  $S = -(1/eT)(L_{yy}^{(0)})^{-1}L_{yy}^{(1)}$ . The converged values of  $\sigma$  and  $S$  are obtained using a dense  $\mathbf{k}$ -point mesh of 121 points along the  $y$  direction. All simulations are carried out at 300 K and a carrier concentration range of  $10^{11}$ – $10^{13}$  cm<sup>-2</sup>.

In general, the relaxation time ( $\tau$ ) is taken to be energy-independent, and obtained by fitting experimental values for pristine bulk materials even in the cases with structural and chemical modifications. However, in principle  $\tau$  is a complex function of the electron energy, temperature, and atomic structure. In this respect, using a  $\tau$  value obtained from pristine graphene is not a reasonable approximation for use in patterned graphene nanoroads, where chemical modification in those samples plays an important role in opening the energy gap, which indirectly relates to the relaxation time. Because the goal of our work is to determine the quantitative effect of functionalization on charge transport, we calculate the relaxation time of functionalized graphene samples with Boltzmann transport theory for a reliable quantitative approximation. Here, we consider only the acoustic phonon scattering, and the relaxation time can be expressed as

$$\frac{1}{\tau(\epsilon_{\mathbf{k}})} = \frac{2\pi k_B T D_{ac}^2}{\hbar A \rho_m v_{ph}^2} \sum_{\mathbf{k}'} \delta(\epsilon_{\mathbf{k}} - \epsilon_{\mathbf{k}'}) \quad (2)$$

where  $k_B$  is the Boltzmann constant,  $D_{ac}$  is the deformation-potential coupling constant,  $\rho_m$  the graphene mass density,  $v_{ph}$  the graphene sound velocity, and  $A$  the area of the sample. The term  $\sum_{\mathbf{k}'} \delta(\epsilon_{\mathbf{k}} - \epsilon_{\mathbf{k}'})/A$  yields the density of states of functionalized graphene. This form highlights the proportionality of the scattering rate to the density of states of the 2D graphene sheet (see Supporting Information).

For calculations of the thermal transport, we employ equilibrium molecular dynamics (MD) simulations as discussed in ref 9, which shows a large  $\kappa$  reduction in functionalized graphene with the use of 2D periodic patterns. The MD

simulations describe well the scattering effects of functionalization on thermal transport in graphene, especially for short-wavelength phonons. However, given the current limits of system size and time scales, our simulations do not capture the contributions of long-wavelength phonons, which are important for thermal transport in graphene, resulting in lower  $\kappa$  values in our simulations by an order of magnitude than measured values. In order to predict  $ZT$ , we modify our computed  $\kappa$  values by adding the long-wavelength phonon contributions from the Klemens model,<sup>27,28</sup> allowing one to obtain approximate  $\kappa$  values for larger graphene samples (see Supporting Information).<sup>9</sup>

**Atomic Structure.** Figure 1a shows a schematic of a 2D thermoelectric device based on graphene nanoroads with armchair-type interfaces formed via partial functionalization. This type of superlattice is modeled with a repeated structure of pristine graphene ( $sp^2$  network) and graphene with functionalization ( $sp^2 + sp^3$  network) within the same sheet, where the former exhibits semimetallic behavior, and the latter shows insulating or semiconducting behavior depending on the functional groups. The electronic structure of functionalized graphene is strongly influenced by the functionalized configurations on the graphene sheet, determined by the shape and chemistry of the functional groups. For example, H-functionalization generates full functionalization (perfect  $sp^3$  network) showing insulating behavior, whereas hydrocarbon chains generate partial functionalization of the graphene sheet due to the steric repulsion between the chains, exhibiting a graphene-like electronic structure with a distorted cone-shaped band. In this work, we consider two different functional groups (H and pentane  $C_5H_{12}$ , referred to as C5) to investigate how chemical functionalization influences the thermoelectric properties of a patterned graphene superlattice.

**H-Functionalized Graphene.** We first compute the electronic structure of partially H-functionalized graphene (HG). The width ( $W$ ) of the pattern in our simulations ranges from 6–23 Å and can be represented by the number of pure carbon dimers ( $N_C$ ) along the pattern direction in the unit cell as shown in Figure 2a. Although graphene is a zero-gap semiconductor with a 2D cone-shape linear energy dispersion, all HG samples show semiconducting behavior with a finite energy gap due to confinement effects of the graphene parts of the structure. As in the case of armchair graphene-based nanoribbons,<sup>29</sup> the gap can be categorized into three different families depending on  $N_C$ :  $E_g(N_C = 3p + 2) \ll E_g(N_C = 3p) < E_g(N_C = 3p + 1)$ , where  $p$  is an integer. This hierarchy is in good agreement with previous work on the energy gaps of hydrogenated graphene superlattices<sup>22,30</sup> and it is also found that  $E_g$  decreases with  $N_C$  values within each family due to decreasing confinement effects. All HG samples show a flattened energy dispersion across the pattern direction, whereas energy bands along the pattern direction ( $\Gamma \rightarrow Y$ ) retain the dispersive nature of pristine graphene, implying quasi-1D transport in such graphene superlattices. The reduction of the charge transport dimension in all HG samples introduces a peak in the DOS near the band edge, which would be expected to enhance  $S$  according to Mahan–Sofa theory.<sup>31</sup>

The relaxation time of HG samples is calculated using eq 2 with density of states from first-principle calculations. Here, the  $D_{ac}$  value of pristine graphene (16 eV)<sup>32</sup> is used for the HG cases, which is a reasonable approximation since charge carriers are confined within the 1D pristine graphene regions as shown in Figure 1b. Figure 2b shows our calculated  $\tau$  for pristine

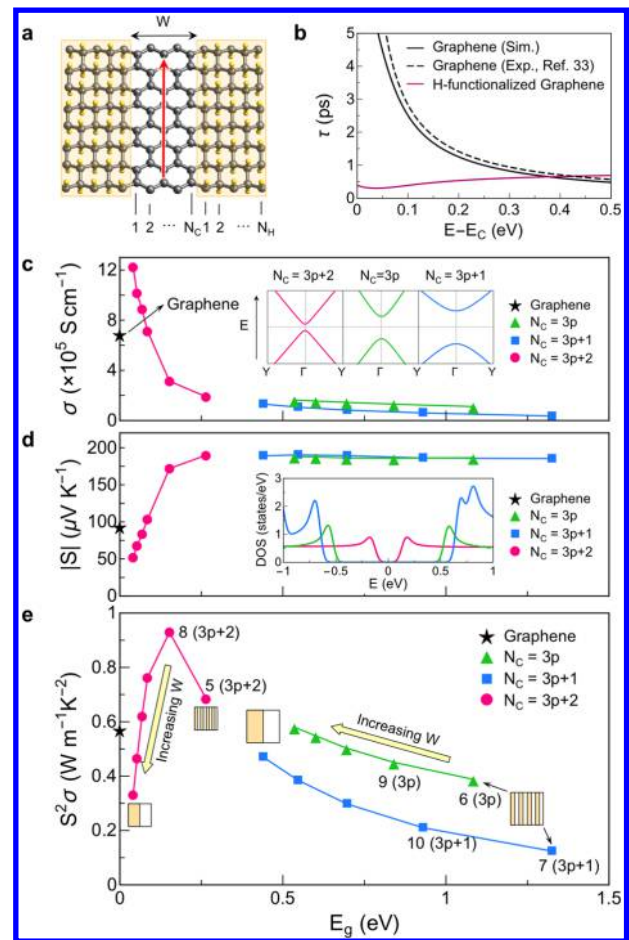


**Figure 2.** (a) Structure of H-functionalized patterned graphene nanoroads along with structural variables. The red arrow represents the direction of transport considered in our work. (b) Relaxation time for graphene and HG as a function of the carrier energy. (c) Electrical conductivities of HG samples as a function of band gap ( $E_g$ ). Inset represents computed energy dispersions of three different HG samples for  $N_C = 3p + 2$  (pink),  $N_C = 3p$  (green) and  $N_C = 3p + 1$  (blue), respectively. (d) Seebeck coefficients of HG samples. Inset represents computed DOS per unit cell. (e) Power factors of HG samples at 300 K. Schematic figures of HG samples for the widest and narrowest pattern widths within each family are shown to highlight the decrease in  $E_g$  with pattern width within each family.

graphene and a HG sample ( $N_C = 6$ ) as a function of the carrier energy. For pristine graphene  $\tau$  decreases with carrier energy, in good agreement with experiments that showed the room-temperature intrinsic resistivity of graphene  $\sim 30 \Omega$  is limited only by intrinsic LA phonon scattering.<sup>33</sup> The scattering becomes more severe in HG samples compared with graphene, particularly near the band edge. We also find that calculated  $\tau$  values in HG samples are proportional to the width of the pattern, resulting in stronger scattering for narrower patterns, similar to the ribbon width dependence in GNR.<sup>34</sup>

The electrical conductivity and Seebeck coefficient, are calculated as a function of carrier concentration ( $n_i$ ), where  $\sigma$  increases with  $n_i$  and  $S$  decreases, resulting in a maximum power factor ( $S^2\sigma$ ) at carrier concentrations ( $n_{peak}$ ) between  $10^{12}$ – $10^{13}$   $cm^{-2}$ , corresponding to the band edge. Our calculated  $\sigma$  and  $S$  values at  $n_{peak}$  as a function of band gap are presented in Figures 2c and d for the range of HG samples considered. Here, we are only interested in thermoelectric properties along the pattern direction because values in the

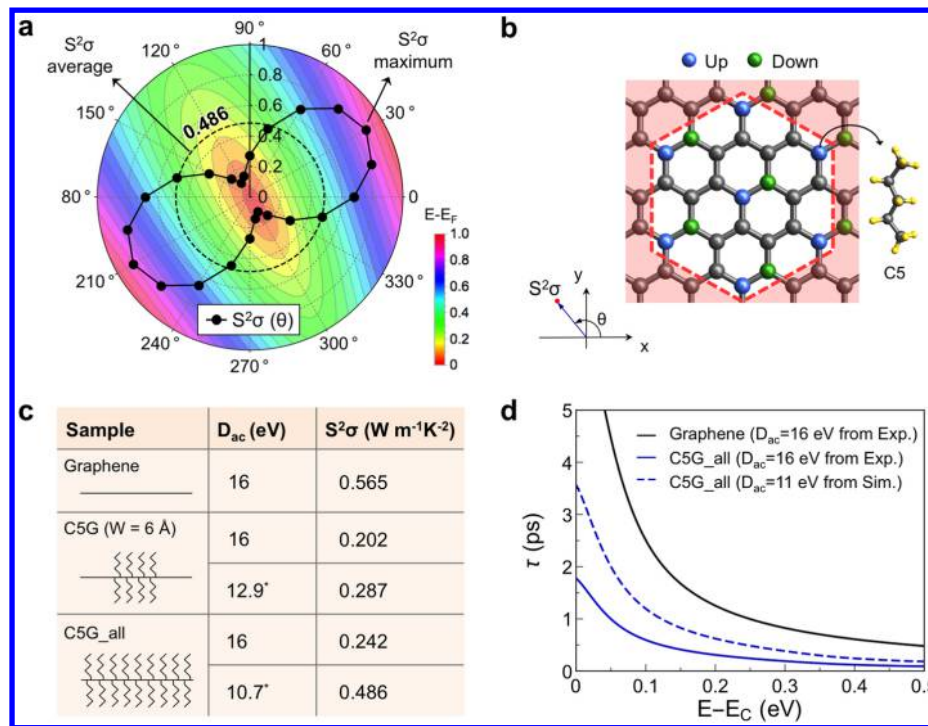


**Figure 3.** (a) Power factor of fully functionalized CSG as a function of spatial direction. The black dashed line indicates the average value of the power factor. The background represents the energy band contour of constant energy, showing a distorted cone-shape dispersion. (b) Configuration of C5-functionalized graphene (CSG) with the structure of C5 (pentane:  $C_5H_{12}$ ). C5 chains are arranged in a two-dimensional hexagonal close-packed lattice on the graphene sheet. (c) Deformation potential constant ( $D_{ac}$ ) and corresponding power factor of CSG samples, where \* represents calculated values for CSG samples. CSG\_all represents a CSG sample with full coverage. Power factor calculated with the  $D_{ac}$  value of pristine graphene (16 eV) are shown for comparison. (d) Relaxation time for CSG as a function of the carrier energy.

direction perpendicular to the pattern are negligible due to the band flattening.

As can be seen in Figure 2c,  $\sigma$  decreases with  $E_g$  implying that wider H-patterns exhibit higher  $\sigma$  because  $\tau$  increases. Clearly, the presence of the H-pattern reduces  $\sigma$  compared to pristine graphene, especially for the  $3p$  and  $3p + 1$  families, due to both the reduced  $\tau$  as well as reduced group velocities. Among the three different families, samples in the  $3p + 1$  family show the lowest  $\sigma$ , which can be explained by the lowest slope in the band dispersion as shown in the inset of Figure 2c. It is interesting to observe that  $3p + 2$  family samples with  $E_g < 0.1$  eV show higher  $\sigma$  than graphene because the maximum power factor arises at a higher carrier concentration, where more carriers contribute to the transport. In contrast to  $\sigma$ , most of the HG samples show larger  $S$  than pristine graphene. This can be explained by a peak in the DOS near the band edge, induced from the reduction of the charge transport dimension as shown in the inset of Figure 2d. This sharp increase in the DOS enhances  $S$  by a factor of 2 for the  $3p$  and  $3p + 1$  family samples. Because  $S$  is proportional to the magnitude of the DOS peak,  $S$  is expected to increase as the pattern width decreases in going from the bulk to the nanostructured case. This is indeed what we observe for the  $3p + 2$  cases. However, for the  $3p$  and  $3p + 1$  family, the maximum power factor occurs at higher carrier concentration for narrower pattern samples, and the decrease of  $S$  due to higher carrier concentration is large enough to compensate the increase of  $S$  due to stronger confinement effects as the pattern width decreases, resulting in nearly constant  $S$  values among samples.

These two conflicting thermoelectric properties produce a strong dependence between the power factor and band gap

(Figure 2e), with a maximum value of  $S^2\sigma$  at  $E_g \sim 0.15$  eV for the HG sample with the  $N_C = 8$  pattern ( $W = 10 \text{ \AA}$ ). For  $E_g > 0.15$  eV,  $S^2\sigma$  decreases as  $E_g$  increases, due to the fact that the wider H-pattern generates superior charge transport in these graphene superlattices. The reduction in  $S^2\sigma$  in this regime is mainly due to more severe scattering for narrower H-patterns. On the other hand,  $S^2\sigma$  decreases as  $E_g$  decreases for  $E_g < 0.15$  eV, and this behavior can be explained by the  $S^2$  term in the power factor, which is significantly reduced with H-pattern width, due to weaker confinement effects. Thus, the HG sample with the  $N_C = 8$  pattern exhibits the best performance for TE applications with  $S^2\sigma \sim 0.93 W m^{-1} K^{-2}$ , which is about 1.6 times larger than pristine graphene. We note that this large enhancement in power factor arises from considerably enhanced  $S$  as well as a comparatively small reduction in  $\sigma$  in spite of strong scattering due to the H-pattern.

**C5-Functionalized Graphene.** We next consider the case of functionalizing graphene with pentane chains (C5), which was shown previously<sup>9</sup> to further reduce  $\kappa$  in graphene superlattices beyond simple hydrogen functionalization due to a clamping effect imposed by the steric hindrance between chains (see Supporting Information). In contrast to the one-dimensional dispersion of HG cases, C5-functionalized graphene (CSG) exhibits a 2D distorted cone-shape band, resulting in an anisotropic  $\sigma$  (Figure 3a). This difference is caused by the fact that C5 patterns cannot generate confinement effects in graphene due to their inability to pack closely enough to functionalize every carbon atom (Figure 3b). As a result, the DOS of a CSG sample is similar to that of pristine graphene (Figure 1c), showing no peak at the band edge, and our computed  $S$  values are similar in all directions to

that of pristine graphene. Among the CSG samples we considered with different pattern widths, the case of fully C5-functionalized graphene (i.e., width = 0, so no “nano-roads”) exhibits the largest  $S^2\sigma$ , with an average value close to the value of pristine graphene ( $0.486 \text{ W m}^{-1} \text{ K}^{-2}$ ). The peak in  $S^2\sigma \sim 0.88 \text{ W m}^{-1} \text{ K}^{-2}$  arises at  $\theta = 30^\circ$ , where the group velocity along this direction is largest due to the distorted band dispersion (Figure 3a).

It should be noted that in contrast to HG samples, charge carriers in CSG samples are not confined in an unfunctionalized region but rather delocalized over the entire 2D graphene sheet as shown in Figure 1b. Accordingly, we need to determine an accurate value of  $D_{ac}$  for CSG samples, which considers the electron–phonon coupling for this specific functionalization. To this end, we compute  $D_{ac}$  using Bardeen and Shockley’s theory,<sup>35</sup> and the calculated  $D_{ac}$  and corresponding power factors are shown in Figure 3c (see Supporting Information). Reduction in  $D_{ac}$  gives rise to an increase in  $\tau$  for the CSG samples, which is inversely proportional to the square of  $D_{ac}$ , as shown in Figure 3b. It is interesting to note that C5-functionalization leads to the suppression of electron–phonon coupling in the graphene sheet, implying diminished charge scattering. Thus, the values of  $S^2\sigma$  for CSG samples are close to the value of graphene, showing potential for TE applications when combined with the significantly reduced  $\kappa$  for this type of functionalization.<sup>9</sup>

For the case of H-functionalization, confinement of the graphene region leads to an enhanced power factor, whereas the confined phonon modes reduce thermal transport along the pattern direction by a factor of 3 compared to pristine graphene.<sup>9</sup> In contrast, C5-functionalization greatly suppresses  $\kappa$  in graphene superlattices from the steric repulsion of the C5 chains,<sup>9</sup> although as shown above, no power factor improvement is observed for this case. Combining *both* functionalizations into the same sample could achieve the best of both worlds: namely, controllable charge transport with H-functionalization and tunable thermal transport with C5-functionalization. In this combined case, a well-defined boundary is formed between the  $sp^2$  graphene and  $sp^3$  domains, giving rise to the same types of electronic confinement effects as in the HG cases, and therefore the same energy dispersions, resulting in significant enhancements in  $S^2\sigma$ . We can also achieve further suppression of  $\kappa$  compared with either the HG or CSG samples due to a combination of boundary scattering and clamping effects.

Using the correction for  $\kappa$  from the Klemens model, we show our calculated thermoelectric properties of patterned graphene nanoroads as a function of functional groups in Figure 4 for the  $N_C = 8$  pattern width. We predict a maximum value of  $ZT \sim 0.09$  for pristine graphene at room temperature, in good agreement with experimental measurements of intrinsic thermoelectric properties for a graphene monolayer without any extrinsic scattering sources (see Supporting Information).<sup>33</sup> By combining the  $\kappa$  reduction and  $S^2\sigma$  enhancements in each sample, we obtain significantly increased  $ZT$  values for all functionalized graphene samples compared to the pristine graphene case. Among these cases, a factor of  $\sim 30$  enhancement in  $ZT$  can be achieved in the C5 + H sample, with corresponding  $ZT$  values as large as 3 at room temperature. This large enhancement in  $ZT$  is due to a combination of a large reduction in  $\kappa$  a 40% enhancement in  $S^2\sigma$  compared to pristine graphene. Interestingly, the fully C5-functionalized graphene case also yields a figure of merit well above 2 at room temperature, even without periodic patterning on the graphene

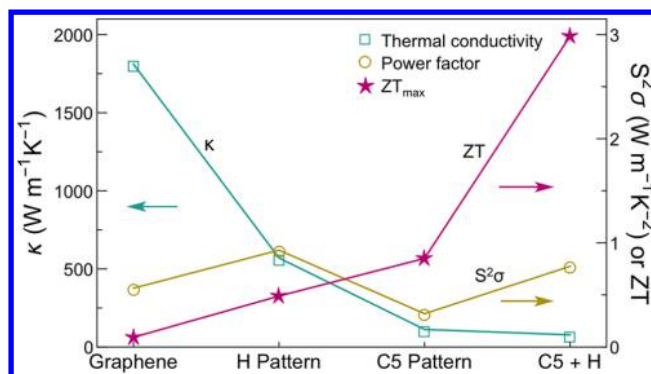


**Figure 4.** Thermoelectric properties of patterned graphene nanoroads with different functional groups at room temperature. Calculated thermal conductivity (green), power factor (orange), and  $ZT$  (red) of patterned graphene along the pattern direction, as a function of functional groups are shown for  $N_C = 8$  pattern width.

sheet, suggesting that chemical functionalization by itself offers further opportunities for graphene to become an appealing TE material without complex nanopatterning. The results suggest that chemical functionalization could be an important route to designing high-efficiency graphene-based TE materials, by allowing for independent control of charge transport and thermal transport.

In this work, we investigated the thermoelectric properties of patterned graphene nanoroads functionalized with H and C5 chains using both classical and quantum mechanical calculations. Periodically patterned  $sp^3$ -hybridized carbon regions on graphene were shown to introduce DOS peaks at the band edge, which lead to substantially enhanced  $S$  and  $S^2\sigma$  compared to that of pristine graphene at carrier concentrations corresponding to the band edge. These results also demonstrate that the thermal transport in such materials can be tuned by functional groups separately from the power factor, which simply depends on the pattern width. We note that unlike the case of standard, 3-dimensional TE materials, for the 2D cases considered here it is not difficult to achieve reduced  $\kappa$  and enhanced  $S^2\sigma$  *simultaneously*, resulting in broad tunability of thermoelectric properties for this class of materials. Finally, although fabrication of functionalized graphene with 100% H coverage or regular C5 chain ordering may be challenging, we note that incomplete H-functionalization in the patterned region has a negligible influence on  $ZT$  values of HG and (C5 + H) – G samples since charge transport in these samples is mainly determined by the condition of the pristine graphene region. Furthermore, our calculations of a fully functionalized CSG sample with random (as opposed to regular) C5 chain ordering still shows high  $ZT$  values at room temperature, as the decrease in thermal conductivity roughly tracks the decrease in the power factor, indicating that perfectly controlled ordering is not crucial for the potential use of functionalized graphene in TE applications.

## ■ ASSOCIATED CONTENT

### 📄 Supporting Information

Additional simulation details on thermal conductivity calculations (molecular dynamics simulations and Klemens model), relaxation time calculations, and thermoelectric coefficient as a function of carrier concentration for pristine graphene, HG, and CSG samples. This material is available free of charge via the Internet at <http://pubs.acs.org>.

## ■ AUTHOR INFORMATION

## Corresponding Author

\*E-mail: jcg@mit.edu.

## Notes

The authors declare no competing financial interest.

## ■ REFERENCES

- (1) Venkatasubramanian, R.; Siivola, E.; Colpitts, T.; O'Quinn, B. *Nature* **2001**, *413*, 597–602.
- (2) Dresselhaus, M. S.; Chen, G.; Tang, M. Y.; Yang, R. G.; Lee, H.; Wang, D. Z.; Ren, Z. F.; Fleurial, J. P.; Gogna, P. *Adv. Mater.* **2007**, *19*, 1043–1053.
- (3) Lee, J. H.; Galli, G. A.; Grossman, J. C. *Nano Lett.* **2008**, *8*, 3750–3754.
- (4) Snyder, G. J.; Toberer, E. S. *Nat. Mater.* **2008**, *7*, 105–114.
- (5) Uher, C. Skutterudites: Prospective novel thermoelectrics. In *Semiconductors and Semimetals*; Tritt, T., Ed.; Academic Press: San Diego, 2001; Vol. 69, p 139–253.
- (6) Heremans, J. P.; Jovovic, V.; Toberer, E. S.; Saramat, A.; Kurosaki, K.; Charoenphakdee, A.; Yamanaka, S.; Snyder, G. J. *Science* **2008**, *321*, 554–557.
- (7) Lee, J. H.; Wu, J. Q.; Grossman, J. C. *Phys. Rev. Lett.* **2010**, *104*, 016602.
- (8) Georgakilas, V.; Otyepka, M.; Bourlinos, A. B.; Chandra, V.; Kim, N.; Kemp, K. C.; Hobza, P.; Zboril, R.; Kim, K. S. *Chem. Rev. (Washington, DC, U.S.A.)* **2012**, *112*, 6156–6214.
- (9) Kim, J. Y.; Lee, J. H.; Grossman, J. C. *ACS Nano* **2012**, *6*, 9050–9057.
- (10) Bolotin, K. I.; Sikes, K. J.; Jiang, Z.; Klima, M.; Fudenberg, G.; Hone, J.; Kim, P.; Stormer, H. L. *Solid State Commun.* **2008**, *146*, 351–355.
- (11) Seol, J. H.; Jo, I.; Moore, A. L.; Lindsay, L.; Aitken, Z. H.; Pettes, M. T.; Li, X. S.; Yao, Z.; Huang, R.; Broido, D.; Mingo, N.; Ruoff, R. S.; Shi, L. *Science* **2010**, *328*, 213–216.
- (12) Zuev, Y. M.; Chang, W.; Kim, P. *Phys. Rev. Lett.* **2009**, *102*, 096807.
- (13) Geim, A. K.; Novoselov, K. S. *Nat. Mater.* **2007**, *6*, 183–191.
- (14) Bolotin, K. I.; Sikes, K. J.; Hone, J.; Stormer, H. L.; Kim, P. *Phys. Rev. Lett.* **2008**, *101*, 096802.
- (15) Balandin, A. A. *Nat. Mater.* **2011**, *10*, 569–581.
- (16) Poudel, B.; Hao, Q.; Ma, Y.; Lan, Y. C.; Minnich, A.; Yu, B.; Yan, X. A.; Wang, D. Z.; Muto, A.; Vashaee, D.; Chen, X. Y.; Liu, J. M.; Dresselhaus, M. S.; Chen, G.; Ren, Z. F. *Science* **2008**, *320*, 634–638.
- (17) Balandin, A. A.; Ghosh, S.; Bao, W. Z.; Calizo, I.; Teweldebrhan, D.; Miao, F.; Lau, C. N. *Nano Lett.* **2008**, *8*, 902–907.
- (18) Vincent, E. D.; Behnam, Ashkan; Conley, Hiram J.; Bolotin, Kirill I.; Pop, a. E. *Nano Lett.* **2013**, *13*, 4581–4586.
- (19) Sun, Z. Z.; Pint, C. L.; Marcano, D. C.; Zhang, C. G.; Yao, J.; Ruan, G. D.; Yan, Z.; Zhu, Y.; Hauge, R. H.; Tour, J. M. *Nat. Commun.* **2011**, *2*, 559.
- (20) Liu, Z.; Ma, L. L.; Shi, G.; Zhou, W.; Gong, Y. J.; Lei, S. D.; Yang, X. B.; Zhang, J. N.; Yu, J. J.; Hackenberg, K. P.; Babakhani, A.; Idrobo, J. C.; Vajtai, R.; Lou, J.; Ajayan, P. M. *Nat. Nanotechnol.* **2013**, *8*, 119–124.
- (21) Wang, Q. H.; Jin, Z.; Kim, K. K.; Hilmer, A. J.; Paulus, G. L. C.; Shih, C. J.; Ham, M. H.; Sanchez-Yamagishi, J. D.; Watanabe, K.; Taniguchi, T.; Kong, J.; Jarillo-Herrero, P.; Strano, M. S. *Nat. Chem.* **2012**, *4*, 724–732.
- (22) Singh, A. K.; Yakobson, B. I. *Nano Lett.* **2009**, *9*, 1540–1543.
- (23) Kresse, G.; Furthmuller, J. *Phys. Rev. B* **1996**, *54*, 11169–11186.
- (24) Kresse, G.; Joubert, D. *Phys. Rev. B* **1999**, *59*, 1758–1775.
- (25) Perdew, J. P.; Wang, Y. *Phys. Rev. B* **1992**, *45*, 13244–13249.
- (26) Madsen, G. K. H.; Singh, D. J. *Comput. Phys. Commun.* **2006**, *175*, 67–71.
- (27) Klemens, P. G. *J. Wide Bandgap Mater.* **2000**, *7*, 332–339.
- (28) Chen, S. S.; Wu, Q. Z.; Mishra, C.; Kang, J. Y.; Zhang, H. J.; Cho, K. J.; Cai, W. W.; Balandin, A. A.; Ruoff, R. S. *Nat. Mater.* **2012**, *11*, 203–207.
- (29) Son, Y. W.; Cohen, M. L.; Louie, S. G. *Phys. Rev. Lett.* **2006**, *97*, 216803.
- (30) Lee, J. H.; Grossman, J. C. *Phys. Rev. B* **2011**, *84*, 113413.
- (31) Mahan, G. D.; Sofo, J. O. *Proc. Natl. Acad. Sci. U.S.A.* **1996**, *93*, 7436–7439.
- (32) Pennington, G.; Goldsman, N.; Akturk, A.; Wickenden, A. E. *Appl. Phys. Lett.* **2007**, *90*.
- (33) Chen, J. H.; Jang, C.; Xiao, S. D.; Ishigami, M.; Fuhrer, M. S. *Nat. Nanotechnol.* **2008**, *3*, 206–209.
- (34) Fang, T.; Konar, A.; Xing, H.; Jena, D. *Phys. Rev. B* **2008**, *78*.
- (35) Bardeen, J.; Shockley, W. *Phys. Rev.* **1950**, *80*, 72–80.